A&A 385, 884–895 (2002)
DOI: 10.1051/0004-6361:20020178

Astronomy & Astrophysics

$BVRIJHK$ photometry of post-AGB candidates[⋆,⋆⋆]

T. Fujii[1,2,⋆⋆⋆], Y. Nakada[1,3], and M. Parthasarathy[2,4]

[1] Institute of Astronomy, University of Tokyo, 2-21-1 Osawa, Mitaka, Tokyo 181-0015, Japan
[2] National Astronomical Observatory of Japan, 2-21-1 Osawa, Mitaka, Tokyo 181-8588, Japan
[3] Kiso Observatory, Institute of Astronomy, University of Tokyo, Mitake, Kiso, Nagano 397-0101, Japan
[4] Indian Institute of Astrophysics, Bangalore 560034, India

Received 27 March 2000 / Accepted 20 December 2001

Abstract. $BVRIJHK$ photometric observations are presented for 27 post-AGB candidates. Almost all objects show a double peaked SED curve in the optical to far-infrared wavelengths. Seventeen objects were classified as post-AGB stars on the basis of their spectral type, location in the IRAS color-color diagram and SED. The physical parameters of the observed post-AGB stars, the inner radius of the detached shell, the mass of the shell and the distance were derived using the simple dust shell model. We compared our observational sequence of post-AGB objects to the theoretical evolutionary sequence (Schönberner 1983; Blöcker 1995) in the stellar temperatures versus age diagram. We found that two post-AGB stars, IRAS 05040+4820 and 08187-1905, have low stellar temperature with a large dynamical age of the dust shell. They appear to provide the first observational evidence that some low-mass stars bypass the planetary nebulae stage because of their slow increase in stellar temperature.

Key words. stars: AGB and post-AGB – stars: circumstellar matter – stars: evolution – stars: mass-loss – infrared: stars – ISM: Planetary Nebulae: general

1. Introduction

Low to intermediate-mass stars cross the HR diagram horizontally from the tip of the asymptotic giant branch (AGB) to the planetary nebula (PN) region after they terminate a rapid mass-loss phase. This transition phase is called post-AGB phase of evolution. From an analysis of the IRAS point source catalog, several post-AGB stars have been identified (Parthasarathy & Pottasch 1986, 1989; Pottasch et al. 1988). The spectral energy distribution (SED) of post-AGB stars is double peaked. One peak is at far-infrared wavelengths due to the cold dust-shell (100–200 K) and the other peak is at shorter wavelengths, optical or near-infrared, from the obscured central star. The cold dust-shell was observed by IRAS. Most of the post-AGB stars, proto-planetary nebulae (PPNe) and PNe were found within the IRAS color box defined by $F(12\ \mu\mathrm{m})/F(25\ \mu\mathrm{m}) < 0.3$ and $F(25\ \mu\mathrm{m})/F(60\ \mu\mathrm{m}) > 0.3$ (van der Veen & Habing 1988; Pottasch et al. 1988). They are well separated from other types of objects. Based on the IRAS color-color diagrams (Pottasch et al. 1988; Preite-Martinez 1988) one can conclude that there is a good chance that an object is a PN, a PPN or a post-AGB star if it is within the box defined by the colors mentioned above. An occasional HII region, Seyfert galaxy or T-Tau star is not excluded from this range.

Like PNe, PPNe are composed of post-AGB central stars and detached circumstellar envelopes of gas and dust; however, unlike PNe, their central stars are too cool to photoionize the envelopes. The terms PPNe and post-AGB stars are often used to describe the objects evolving from the tip of the AGB to PNe. Often one uses the term PPNe to describe the circumstellar shells of post-AGB stars that are not yet photoionized.

Since the post-AGB objects span a wide range in the spectral type of their central star as well as the obscuration of their dust shell, the analysis of their SED needs a combination of the optical and near-infrared photometry

Send offprint requests to: T. Fujii,
e-mail: takahiro.fujii@nao.ac.jp

⋆ Based on observations obtained at Kiso Observatory, Nagano, Japan.

⋆⋆ Table 2 is also available in electronic form at the CDS via anonymous ftp to cdsarc.u-strasbg.fr (130.79.128.5) or via
http://cdsweb.u-strasbg.fr/cgi-bin/qcat?J/A+A/385/884

⋆⋆⋆ *Present address*: Faculty of Science, Kagoshima University, 1-21-35 Korimoto, Kagoshima 890-0065, Japan.

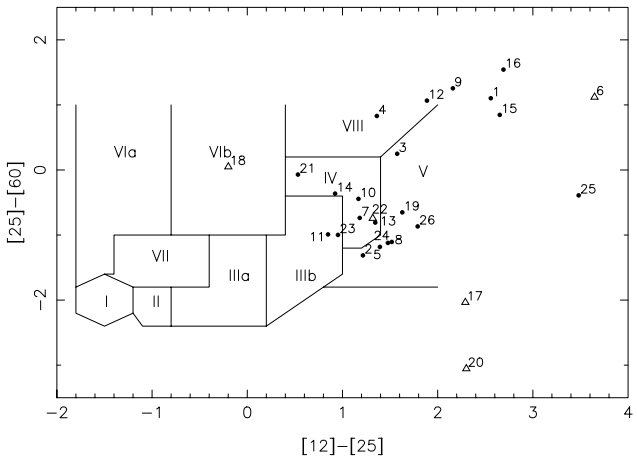

Fig. 1. The positions of program IRAS sources in the van der Veen & Habing (1988) IRAS color-color diagram. The IRAS colors are defined as $[12]-[25] = 2.5\log(F_{25\,\mu m}/F_{12\,\mu m})$, $[25]-[60] = 2.5\log(F_{60\,\mu m}/F_{25\,\mu m})$. Filled circles denote objects which have IRAS quality index 3 or 2 at 12 μm, 25 μm and 60 μm. Open triangles denote objects which have qindex 1 in one of the 12 μm, 25 μm and 60 μm bands.

in addition to the IRAS data. In order to understand the nature of the SED in the shorter wavelength, optical and near-infrared photometry has been performed for some of the post-AGB stars. Manchado et al. (1989) and García-Lario et al. (1990, 1997) carried out JHK photometric survey of several IRAS sources with colors like PNe. The SEDs of eight post-AGB candidates were studied based on $BVRIJHK$ photometry by Hrivnak et al. (1989). They showed that multi-color photometry in combination with spectral types of the IRAS sources enables one to estimate the parameters of the stars and their circumstellar dust envelopes.

In order to increase the number of well-determined post-AGB stars and to classify them using SEDs from optical to far-infrared wave length, we have initiated a program to carry out systematic optical and near-infrared photometry of post-AGB candidates. We have selected several post-AGB candidates based on the above IRAS colors that are observable from Kiso Observatory. In this paper we report the $BVRIJHK$ photometric observations and analysis of 27 post-AGB candidates.

2. Observations and analysis

Photometric observations in $BVRIJHK$ were made using the CCD and infrared cameras at Kiso Observatory, University of Tokyo. The list of post-AGB candidates together with their IRAS fluxes are given in Table 1. The location of the sources in the IRAS color-color diagram is shown in Fig. 1. The observational results are tabulated in Table 2.

2.1. Optical observation and data reduction

The optical photometric observations were performed using a 105 cm Schmidt telescope with a CCD camera. The CCD camera contains a TI Japan TC215 chip with an array size of 1024 × 1024 pixels. The field of view is about 12′.5 × 12′.5 and one pixel is 0″.75 in the sky. The CCD images were taken at B, V, R_C and I_C filters. The raw data were processed using the IRAF image data reduction software by subtracting bias and dividing by the dome flat field. We used the DoPHOT (Schechter et al. 1993) program to obtain magnitudes. The instrumental magnitudes were transformed to the Johnson-Cousins photometric system magnitudes by analyzing the frames of standard stars from Landolt (1992). The derived B, V, R_C and I_C magnitudes are shown in Table 2 Cols. 3, 4, 5 and 6. The observational date is shown in Table 2 Col. 10.

2.2. Near-infrared observation and data reduction

The near-infrared photometric observations were carried out using J, H and K_S filters. The K_S filter has a shorter cut-off wavelength in order to reduce the contribution of the thermal background radiation. The passband of K_S is from 2.0 to 2.3 μm. KONIC (Kiso Observatory near-infrared camera, Itoh et al. 1995) with a 1040 × 1040 elements PtSi Schottky-barrier array (Mitsubishi Electric Co.) was attached to the 105 cm Schmidt telescope. The field of view is about 18′.4 × 18′.4. Standard data processing (dark subtraction and flat-fielding)was performed with the IRAF software package. The frames for flat-fielding were made by combining object frames with median filters in the JHK_S band. We used the IRAF/APPHOT package to obtain magnitudes. Several standard stars in the Elias list (Elias et al. 1982) were used to correct for atmospheric absorption and to transform the instrumental magnitudes to the CTIO system. The derived J, H and K magnitudes are shown in Table 2 Cols. 7, 8 and 9. The observational date is shown in Table 2 Col. 11.

2.3. Reddening correction

In order to derive the parameters of the stars, we need to estimate the reddening in the line of sight of these sources. First, we used two methods to obtain reddening: (1) from spectral types of stars, (2) from interstellar extinction maps. While one can estimate both interstellar and circumstellar reddening by using the first method, one can obtain interstellar reddening alone by using the latter method.

Method (1): A_{V1}; for most post-AGB candidates, their spectral types are available in the literature. From the spectral type of the star we know the intrinsic $(B-V)_0$, and from the observed $(B-V)_{obs}$ we estimated the reddening $E(B-V)$ $(= (B-V)_{obs} - (B-V)_0)$. To derive the A_V value, we adopted $R_V = 3.1$, i.e. $A_V = 3.1 \times E(B-V)$.

Table 1. Infrared properties of candidates from IRAS-PSC.

ID No.	IRAS Name	Association SAO or HD	$F_{12\,\mu m}$ [Jy]	$F_{25\,\mu m}$ [Jy]	$F_{60\,\mu m}$ [Jy]	$F_{100\,\mu m}$ [Jy]	VAR[a]	l[b] [deg.]	b[b] [deg.]	qindex[c]
1	02086+7600		0.25	2.68	7.41	10.49	9	127.9	14.2	3333
2	02143+5852		5.90	18.06	5.39	8.97	94	133.9	−1.9	3331
3	02528+4350		0.56	2.38	3.00	2.22	0	145.4	−13.3	3333
4	04269+3550		2.83	9.92	21.29	15.58	19	164.9	−8.6	3333
5	04296+3429		12.74	45.94	15.45	9.22	11	166.2	−9.1	3331
6	05040+4820	SAO 40039	0.25	7.20	20.20	11.00	–	159.8	4.8	1333
7	05089+0459		7.37	21.89	11.10	3.78	14	196.3	−19.5	3333
8	05113+1347		3.78	15.30	5.53	1.67	10	188.9	−14.3	3331
9	05170+0535	SAO 112630	0.60	4.42	14.06	9.38	31	196.8	−17.5	3333
10	05238−0626		0.59	1.74	1.16	1.87	0	208.9	−21.8	3321
11	05341+0852		4.51	9.85	3.96	8.01	0	196.2	−12.1	3331
12	05355−0117	HD 290764	0.68	3.89	10.38	9.00	0	205.5	−16.9	3333
13	05381+1012		0.85	2.93	1.39	9.44	13	195.5	−10.6	3331
14	06013−1452		1.86	4.34	3.11	1.25	0	221.2	−17.2	3331
15	06059−0632	SAO 132875	0.38	4.41	9.64	6.52	12	213.9	−12.5	3322
16	06060+2038	HD 252325	2.27	27.08	112.3	18.39	15	189.8	0.4	3321
17	06284−0937	SAO 133356	0.32	2.60	0.40	369.1	–	219.3	−8.9	1311
18	06338+5333	SAO 25845	0.46	0.38	0.40	1.15	3	162.0	19.6	3211
19	06530−0213		6.11	27.41	15.05	4.10	8	215.4	−0.1	3333
20	07077−1825		0.80	6.66	0.40	211.4	0	231.5	−4.4	3311
21	07131−0147		2.59	4.22	3.96	3.68	1	217.4	4.5	3333
22	07171+1823		0.41	1.38	0.70	1.00	–	199.5	14.4	1331
23	07253−2001		6.30	15.16	6.05	8.05	8	234.9	−1.5	3331
24	07430+1115		7.68	29.93	10.67	2.53	9	208.9	17.1	3333
25	08187−1905	HD 70379	0.71	17.62	12.31	3.68	0	240.6	9.8	3333
26	23304+6147		11.36	59.07	26.60	30.89	8	113.9	0.6	3331
27	(BD+39°4926)	SAO 72704	–	–	–	–	–	98.4	−16.7	–

Notes: BD+39°4926 has no IRAS data.
[a] VAR: percent likelihood of variability.
[b] l, b: Galactic longitude and latitude, respectively.
[c] qindex: Flux density quality (1 = upper limit, 2 = moderate quality, 3 = good quality). From left to right, each figure stand for IRAS photometric band 12 μm, 25 μm, 60 μm and 100 μm.

For the objects whose spectral subclass and/or luminosity class were not determined, we assume a moderate one. The values of intrinsic $(B-V)_0$ and stellar effective temperature $T_{\rm star}$ were quoted from the lists of Schmidt-Kaler (1982). The A_{V1} values contain the contribution from the interstellar and circumstellar reddening.
Method (2): A_{V2}; we estimated A_V values using their galactic latitudes and longitudes and corresponding interstellar extinction maps (Neckel & Klare 1980; Burstein & Heiles 1982; Schlegel et al. 1998).

The spectral type, chemical type (carbon-rich or not), $T_{\rm star}$, $E(B-V)$, two values of A_V (A_{V1} and A_{V2}) and the object type cited from the literature are given in Table 3. In general one can estimate the circumstellar reddening from these two values of A_V. However, for some stars, the A_{V2} (interstellar) is larger than the A_{V1} (interstellar plus circumstellar). This contradiction may be due to uncertainty of interstellar extinction maps and uncertainty of circumstellar extinction law. This may also be due to uncertainty in spectral types in some cases. In particular the A_V value derived from the map depends on the distance to the star and the spatial resolution of these maps is not sufficiently high. Therefore, it is dangerous to blindly accept the A_V value obtained from the map in some cases. Indeed, we could not find dust shell parameters for some stars if we fixed the value of interstellar extinction and the stellar temperature simultaneously. For this reason, we did not adopt A_{V2} to plot SED diagrams and model calculations. We estimated interstellar reddening from model calculations, treating extinction as a parameter. We describe how to estimate interstellar A_V in Sect. 3.

We adopted A_{V1} in plotting optical and near-infrared color-color diagrams to see positions of dereddened post-AGB central stars. We have corrected the photometric

Table 2. Photometric observations of Post-AGB candidates.

ID No.	IRAS Name	B [mag]	V [mag]	R_C [mag]	I_C [mag]	J [mag]	H [mag]	K [mag]	Obs. date Optical	Obs. date NearIR
1	02086+7600					13.54	12.74	>11.14		Oct. 19/1997
2	02143+5852	14.96	13.74	12.96	12.15	10.58	9.51	8.79	Jan. 11/1996	Oct. 19/1997
3	02528+4350	11.11	10.82	10.67	10.46	10.20	9.99	9.62	Jan. 11/1996	Oct. 19/1997
4	04269+3550					12.00	9.65	8.35		Oct. 19/1997
5	04296+3429	16.18	14.17	12.89	11.65	9.67	8.80	8.44	Dec. 02/1995	Feb. 24/1997
		16.41	14.23	12.98	11.74	9.55	8.68	8.28	Dec. 12/1995	Nov. 11/1997
6	05040+4820	10.14	9.58	9.20	8.81	8.24	8.03	7.91	Dec. 02/1995	Oct. 19/1997
		10.12	9.54	9.20	8.86				Dec. 12/1995	
7	05089+0459	16.20	14.48	13.12	11.65	10.14	9.26	8.92	Feb. 07/1996	Feb. 24/1997
						10.09	9.12	8.84		Oct. 17/1997
8	05113+1347	14.67	12.40	11.27	10.26	8.96	8.43	8.05	Dec. 02/1995	Feb. 24/1997
		14.76	12.49	11.32	10.35	9.02	8.44	8.25	Dec. 12/1995	Oct. 17/1997
9	05170+0535	9.72	9.11	8.77	8.44				Dec. 02/1995	
		9.76	9.18	8.83	8.50				Dec. 12/1995	
10	05238−0626	10.96	10.52	10.23	9.94	9.61	9.31	9.03	Dec. 02/1995	Oct. 19/1997
11	05341+0852	15.44	13.58	12.43	11.44	9.97	9.36	9.05	Dec. 02/1995	Nov. 11/1997
		15.53	13.63	12.51	11.49				Dec. 12/1995	
12	05355−0117	10.16	9.81	9.61	9.32				Mar. 06/1996	
13	05381+1012	11.50	10.59	10.04	9.52	8.80	8.44	8.18	Dec. 02/1995	Oct. 19/1997
		11.47	10.57	10.02	9.52				Dec. 13/1995	
14	06013−1452	10.34	10.22	10.17	10.02	9.87	9.72	9.34	Mar. 06/1996	Mar. 24/1997
15	06059−0632	9.33	8.84	8.59	8.30				Mar. 06/1996	
16	06060+2038	11.36	10.76	10.32	9.91				Mar. 06/1996	
17	06284−0937	9.42	8.99	8.78	8.53				Feb. 07/1996	
18	06338+5333	9.32	8.87	8.57	8.25				Dec. 12/1995	
19	06530−0213	16.26	13.99	12.63	11.41				Feb. 07/1996	
20	07077−1825	11.25	10.78	10.43	10.12				Jan. 11/1996	
21	07131−0147	16.40	14.53	13.03	11.58	9.78	9.09	8.30	Dec. 13/1995	Feb. 26/1997
22	07171+1823	12.70	12.73	12.62	12.74				Jan. 11/1996	
23	07253−2001	14.07	13.34	12.82	12.32				Dec. 13/1995	
24	07430+1115	14.22	12.38	11.38	10.50	8.95	8.29	7.87	Dec. 12/1995	Feb. 26/1997
25	08187−1905	9.70	9.03	8.56	8.20				Dec. 13/1995	
26	23304+6147	15.65	13.19	11.80	10.49	8.54	7.86	7.54	Feb. 07/1996	Oct. 19/1997
27	(BD+39°4926)	9.46	9.25	9.07	8.90	8.50	8.36	8.19	Nov. 29/1995	Oct. 19/1997

Notes. The errors of magnitude are $\pm 0\overset{m}{.}08$ for B, $\pm 0\overset{m}{.}05$ for V, R_C and I_C, $\pm 0\overset{m}{.}06$ for J, $\pm 0\overset{m}{.}04$ for H, $\pm 0\overset{m}{.}20$ for K. On Oct. 19/1997, the errors of JHK are $\pm 0\overset{m}{.}18$, $\pm 0\overset{m}{.}12$ and $\pm 0\overset{m}{.}38$, respectively. On Feb. 26/1997 and Mar. 24/1997, they are $\pm 0\overset{m}{.}15$, $\pm 0\overset{m}{.}06$ and $\pm 0\overset{m}{.}20$, respectively. The errors were determined by the magnitude deviations of standard stars. The large errors of near infrared is due to bad sky conditions. The large error in K band may be due to the thermal emission from inside of Schmidt telescope.

data for interstellar and circumstellar reddening using standard extinction laws derived by Rieke & Lebofsky (1985). For R_C and I_C bands, we interpolated values given in the mentioned above paper and adopted them. Strictly, it is not correct to apply a standard extinction law to correct for circumstellar extinction since these two (interstellar and circumstellar) extinction laws are not guaranteed to be the same. However, little is known about circumstellar extinction laws. Therefore, we presumed interstellar and circumstellar extinction laws to be similar here.

The objects for which the evolutionary status is not clear were excluded from further analysis and discussion. The IRAS name of these excluded objects are 02086+7600, 02528+4350, 04269+3550, 05170+0535, 05355−0117, 06013−1452, 06059−0632, 06060+2038, 06284−0937 and 07077−1825. The reasons for excluding

Table 3. Central star's properties and extinction properties.

ID No.	IRAS Name	Spectral Type	Chem.[a] Type	$T_{\rm star}$ [K]	$(B-V)_0$ [mag]	$(B-V)_{\rm obs}$ [mag]	$E(B-V)$ [mag]	A_{V1} [b] [mag]	A_{V2} [c] [mag]	ref.[d]	Object type
1	02086+7600										YSO?
2	02143+5852	F(5Ib[e])		6900	0.33	1.22	0.89	2.75	2.0	A	P-AGB
3	02528+4350										Galaxy
4	04269+3550										YSO?
5	04296+3429	G0Ia	C	5550	0.75	2.07	1.32	4.10	2.23	B	P-AGB
6	05040+4820	A4Ia		8750	0.07	0.57	0.50	1.55	1.0	C	P-AGB
7	05089+0459	M(0Ib[e])		3650	1.64	1.73	0.09	0.27	0.37	A	P-AGB
8	05113+1347	G8Ia	C	4590	1.17	2.27	1.10	3.41	1.67	B	P-AGB
9	05170+0535	G0Ve								D	PMS
10	05238−0626	F2II		7380	0.30	0.44	0.14	0.44	0.37	E	P-AGB
11	05341+0852	F4Iab	C	7060	0.29	1.88	1.59	4.93	1.21	F	P-AGB
12	05355−0117	A5III								G	δ Scuti?, Herbig Ae?
13	05381+1012	G(2Ib[e])		4850	0.86	0.90	0.04	0.13	1.30	B	P-AGB
14	06013−1452	Ae								G	Herbig Ae/Be
15	06059−0632	B3								G	PMS
16	06060+2038	B1V								G	H II region
17	06284−0937	B3ne								H	Herbig Ae/Be
18	06338+5333	F7IVw		6250	0.50	0.45	−0.05	0.0[f]	0.31	G	P-AGB
19	06530−0213	F0Iab	C	7700	0.17	2.28	2.11	6.53	2.0	G	P-AGB
20	07077−1825	O6								G	H II region
21	07131−0147	M5III		3330	1.63	1.87	0.24	0.76	2.0	I	P-AGB, Bipolar-PPN
22	07171+1823	B(5Ib[e])		13600	−0.10	−0.04	0.06	0.19	0.25	J	P-AGB
23	07253−2001	F5Ie		6900	0.33	0.73	0.40	1.23	1.0	E	P-AGB
24	07430+1115	G5 0−Ia	C	4850	1.03	1.84	0.81	2.50	0.06	K	P-AGB
25	08187−1905	F6Ib/II		6630	0.42	0.67	0.25	0.78	0.33	G	P-AGB
26	23304+6147	G2Ia	C	5200	0.87	2.46	1.59	4.93	2.2	B	P-AGB
27	BD+39°4926	B8(Ib[e])		11200	−0.04	0.22	0.26	0.79	0.37	G	P-AGB

[a] C: carbon-rich object.
[b] Derived from intrinsic and observed $B-V$, it contains interstellar and circumstellar extinction.
[c] Derived from interstellar extinction maps.
[d] References for spectral types; (A) Meixner et al. (1999), (B) Hrivnak (1995), (C) Hardorp et al. (1959), (D) Zuckerman et al. (1995), (E) Reddy and Parthasarathy (1996), (F) Parthasarathy (1993), (G) SIMBAD database, (H) van den Ancker et al. (1998), (I) Scarrott et al. (1990), (J) Vijapurkar et al. (1998), (K) Hrivnak and Kwok (1999).
[e] Assumption.
[f] We assumed $A_V = 0.0$, since $(B-V)_{\rm obs} < (B-V)_0$.

these objects from the list of post-AGB candidates are given in Sect. 4.2 (notes on individual objects).

Figures 2 and 3 show the location of the program stars in the $(J-H)_0$, $(H-K)_0$ and $(B-V)_0$, $(V-I)_0$ color-color diagram with the sequence of super-giants (Cox 2000), respectively. The position of the stars in the color-color diagrams indicate the consistency of optical, near-infrared colors and spectral types.

3. Model fitting

In order to derive the dust shell parameters of each object, we introduce a simple model consisting of a central star and a detached shell. The entire SED is given by:

$$F_{\lambda,\rm model} = F_{\lambda,\rm star} + F_{\lambda,\rm shell}\,, \tag{1}$$

where $F_{\lambda,\rm star}$ is flux from the star and $F_{\lambda,\rm shell}$ is flux from the dust shell. We assume that the dust shell is spherically symmetric. The geometrical thickness of the dust shell was taken as 4.7×10^{17} cm, corresponding to 10 000 yr for the duration of AGB mass-loss (superwind mass-loss) with an expansion velocity of $15\,{\rm km\,s^{-1}}$ and a constant mass loss rate.

The central star was assumed to be a blackbody source with a temperature $T_{\rm star}$ and the luminosity $L = 8000\,L_\odot$. The core-mass luminosity relation gave 0.625 $M_\odot$ for the mass of the central star (Blöcker 1995), if we neglect the very thin envelope around the core. Flux from the star is given by:

$$F_{\lambda,\rm star} = \pi B_\lambda(T_{\rm star})\exp(-\tau_{\rm shell,\lambda})\,R_{\rm star}^2/D^2, \tag{2}$$

where $B_\lambda(T_{\rm star})$ is a blackbody function at a wavelength λ, $T_{\rm star}$ is the stellar temperature, $\tau_{\rm shell,\lambda}$ is the optical depth of the dust shell at a wavelength λ, $R_{\rm star}$ is the radius of the star and D is the distance to the star.

A constant expansion velocity of the AGB shell ($V_{\rm exp} = 15\,{\rm km\,s^{-1}}$) and constant mass-loss rate in the AGB phase are assumed. In this case, the mass density in

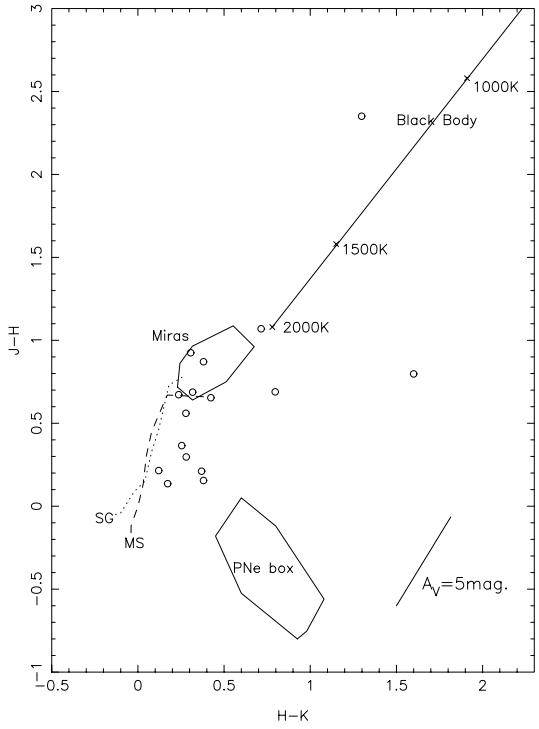

Fig. 2. $(J-H)_0$ vs. $(H-K)_0$ color-color diagram of the 12 observed IRAS sources. We used average magnitudes for the objects which were observed twice. We corrected the interstellar and circumstellar reddening for all stars. Blackbody at temperatures ranging from 2000 to 1000 K are marked on the solid line. The dotted line shows the super-giant (SG) sequence and the dashed line shows the main-sequence (MS) (Cox 2000). The location of Miras and PNe (Glass & Feast 1982; Whitelock 1985) in the color-color diagram are also indicated.

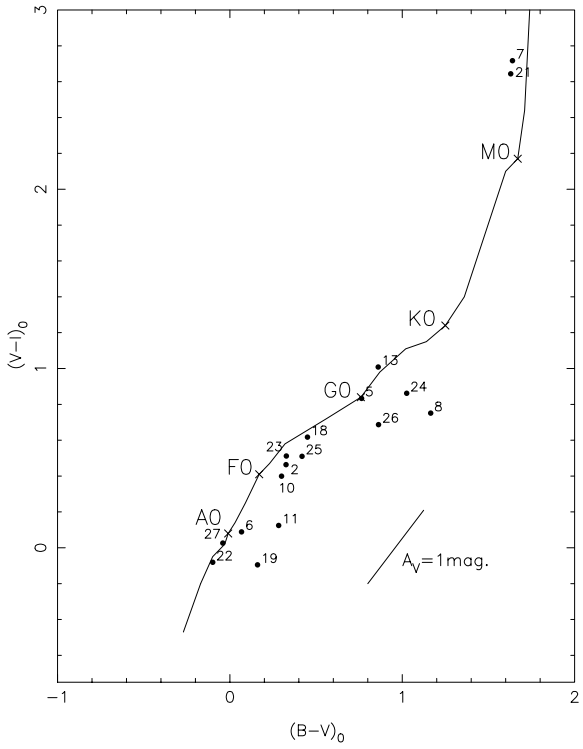

Fig. 3. $(B-V)_0$ vs. $(V-I)_0$ color-color diagram of the 17 observed IRAS sources. We used average magnitudes for the objects which were observed twice. The thick line indicates the color-color sequence of super-giants (Cox 2000).

the shell is inversely proportional to the square of distance from the central star. The number density distribution of dust grains is given by:

$$N_{\rm dust}(r) = N_0 \left(\frac{R_{\rm in}}{r}\right)^2, \tag{3}$$

where N_0 is the number density of dust grains at the inner boundary of the shell ($=R_{\rm in}$) and r is the radial distance from the center of the star.

We assume the shell is optically thin at all wavelengths and the dust grains are in thermal equilibrium with the radiation from the central star. Light scattering by the dust grains is neglected. Frequency dependence of the dust grain absorption cross-section is assumed as a power-law function of wavelength, which allows an analytical form of the temperature distribution of the dust grains. For the dust grain parameters, we assumed the average grain radius $a = 0.1\,\mu$m and the mass density of the grains $\rho_{\rm dust} = 2.5\,{\rm g\,cm^{-3}}$ and absorption efficiency $Q(\lambda) = 0.2/\lambda\,[\mu{\rm m}]$. The temperature distribution is given by:

$$T_{\rm dust}(r) = \left(\frac{R_{\rm star}}{2r}\right)^{\frac{2}{5}} T_{\rm star}\,. \tag{4}$$

Flux from one dust particle at r is given by:

$$F_{\lambda,{\rm dust}.1} = \pi B_\lambda\,(T_{\rm dust}(r))\;Q(\lambda)\,a^2/D^2. \tag{5}$$

Integrating from the inner boundary to the outer boundary of flux of all dust particles, flux from the shell is given by:

$$F_{\lambda,{\rm shell}} = \int_{R_{\rm in}}^{R_{\rm out}} F_{\lambda,{\rm dust}.1}\,N_{\rm dust}(r){\rm d}r\,. \tag{6}$$

In the fitting process, we fixed the stellar temperature $T_{\rm star}$ (we used the same values in Table 3). Therefore fitting parameters are $R_{\rm in}$, $M_{\rm dust}$ and D in our model. In addition to these parameters, interstellar extinction A_V was also treated as a parameter, as mentioned in Sect. 2.3. Changing these four input parameters, we calculated SEDs and we determined the parameters at a minimum of difference between the model and the observation.

We set the dust-to-gas mass ratio to be 5.0×10^{-3}. The dust temperature $T_{\rm dust}$ is determined at the inner boundary of the dust shell. Derived parameters of post-AGB candidates are shown in Table 4. The interstellar extinction-corrected SEDs with a model fitting curve are shown in Figs. 4 and 5.

The IRAS data points for which flux density quality was equal to 1 were not used for fitting. BD+39°4926 was not included since it is not a IRAS source. For IRAS 02143+5852, near-infrared data points were not used for calculation because of the near-infrared excess.

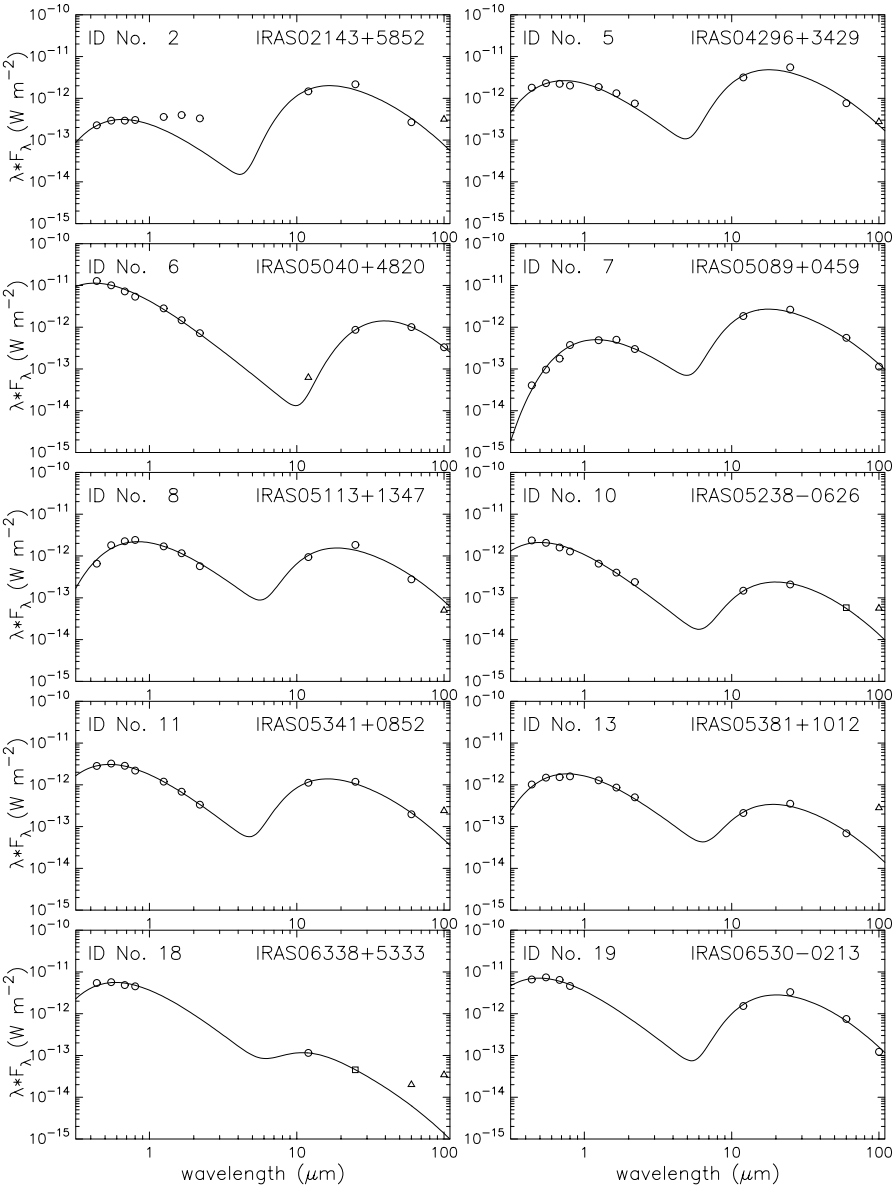

Fig. 4. Reddening-corrected (using A_V values in Table 4) spectral energy distribution of program stars. The full line indicates the calculated SED curve using parameters in Table 4. Open boxes denote IRAS flux density quality = 2 and open triangles indicate IRAS flux density quality = 1. Continued in Fig. 5.

The fitting parameter $R_{\rm in}$ is transformed to $t_{\rm dyn}$, the dynamical time of the dust shell, by being divided by the assumed expansion velocity of the dust shell. While an average value of $V_{\rm exp} = 15\,{\rm km\,s^{-1}}$ is used, the observed values in PPNe are found over some range, for example from 10 to 20 $\rm km\,s^{-1}$ (Hu et al. 1994), and this is translated into an uncertainty in the dynamical time of the dust shell. $M_{\rm dust+gas}$ in Col. 6 of Table 4 is obtained from $M_{\rm dust}$ divided by the dust-to-gas mass ratio. We assume the duration time of AGB mass-loss phase is to be 10 000 yr, therefore one can easily derive the mass-loss rate in AGB phase by dividing $M_{\rm dust+gas}$ by 10^4 yr.

Distances of post-AGB candidates were also estimated using the equation $M_V = (V - A_V) + 5 - 5\log d$ and $M_V = M_{\rm bol} - {\rm B.C.}$ For all the post-AGB candidates, we used $M_{\rm bol} = -5.12$ which correspond to 8000 $L_\odot$. The value of the bolometric correction B.C. of each object was quoted from Schmidt-Kaler (1982) according to its spectral type. The A_V values used are given in Table 3 (A_{V1}). The last column of Table 4 shows estimated distances. The values of D calculated by two different methods agree within a factor of 1.5 except for IRAS 05089+0459. The observed optical to near-infrared energy distribution of this object is very similar to that of an early M star, requiring little extinction A_{V1} for this star. A strong contrast between the small extinction and the large far-infrared excess suggests an oblique torus or disk model for IRAS 05089+0459, but further observations are needed to confirm this hypothesis.

Carbon-rich objects show large differences between the two extinction values A_{V2} and A_{V3} (Table 4). We found that the carbon-rich objects all have a large A_V. One possible explanation is that the circumstellar extinction law of the carbon-rich dust shell is very different from the assumed one, and another possibility is, as in the case of IRAS 05089+0459, the shape of the dust shell deviates from spherical symmetry.

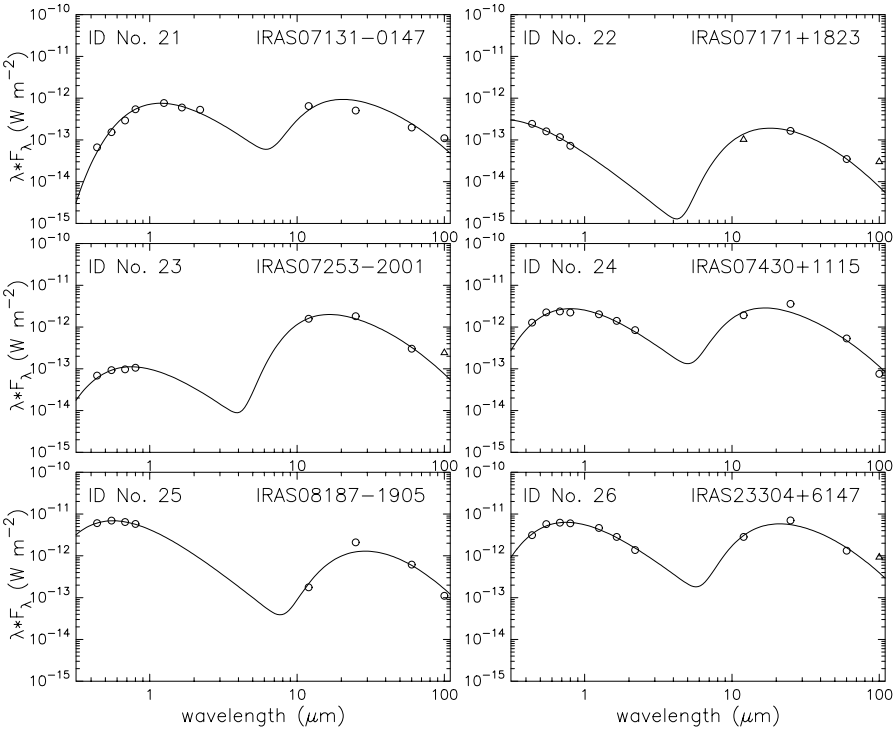

Fig. 5. SED of program stars. The same as Fig. 4.

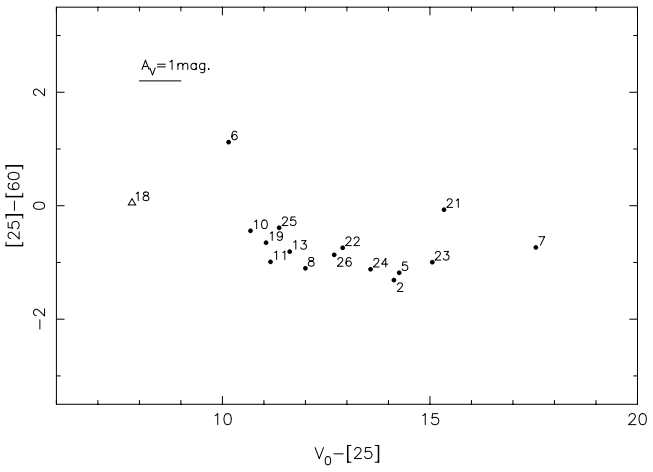

Fig. 6. $V_0-[25]$ vs. [25]–[60] color-color diagram of the 16 observed IRAS sources which are post-AGB objects. Horizontal and vertical axes mean $V_0 + 2.5\log(F_{25\,\mu m})$ and $2.5\log(F_{60\,\mu m}/F_{25\,\mu m})$, respectively. V_0 means V-band magnitude minus A_{V1} in Table 3. Open triangles have large position uncertainty (IRAS flux density quality = 1).

4. Discussion

4.1. Comparison of the stellar temperature with dynamical time of the dust shell

The observed stars have double peaked SEDs, suggesting the existence of the detached cold shell around the central star. Our model calculations actually showed the $R_{\rm in}$ larger than 1.5×10^{16} cm, about 100 times larger than the usual radial size of the dust-forming region of the AGB stars. Similar values were estimated by Hrivnak et al. (1989). As expected from the variety of relative strength of the infrared peak to the visible one, the optical thickness of the dust shell changes from object to object. Figure 6 shows the observed stars on the $V_0-[25]$ to $[25]-[60]$ diagram. A sequence of stars along the horizontal axis in the right part of the diagram presents the change of the optical depth of the shell.

Figure 7 compares the stellar temperature with the dynamical time of the dust shell. The theoretical evolutionary tracks of the post-AGB stars with different core masses by Schönberner (1983) and Blöcker (1995) are plotted in Fig. 7. A common feature of all those theoretical tracks is that the detached shell appears when the stellar temperature goes up to 5000 or 6000 K. This means that they assumed AGB superwind mass-loss ($\dot{M} \sim 10^{-4}\ M_\odot\ {\rm yr}^{-1}$) terminates at these temperatures. In general, the agreement between the observational results and the theoretical evolutionary tracks is satisfactory. However, the observations appear to fit with a somewhat lower core mass indicating a somewhat lower luminosity than that used in the models. Six objects among our samples are distributed below the line of $M_{\rm core} = 0.546\ M_\odot$; two of them, IRAS 05089+0459 and 07131−0147, are peculiar M type stars while the remainders are all G type. The temperatures we used here were cited from different authors and there are uncertainties in the spectral sub-class. Overall, our observational results are in agreement with the theoretical post-AGB models (Fig. 7) (Blöcker 1995; Schönberner 1983). The same kind of figures are shown by van der Veen et al. (1989) and Schönberner & Blöcker (1993). Figure 7 is consistent with their figures.

Table 4. Derived fitting parameters of each Post-AGB candidate.

ID No.	IRAS Name	$T_{\rm star}$[a] [K]	$T_{\rm dust}$ [K]	$t_{\rm dyn}$ [yr]	$M_{\rm dust+gas}$[b] [$M_\odot$]	A_{V3}[c] [mag]	$D_{\rm fit}$[d] [pc]	D_{M_V}[e] [pc]
2	02143+5852	6900	205	338	0.740	1.66	16 900	16 400
5	04296+3429	5550	193	354	0.420	4.36	7090	10 200
6	05040+4820	8750	97	2460	0.254	1.31	4010	3930
7	05089+0459	3650	189	303	1.08	1.18	13 900	40 500
8	05113+1347	4590	185	358	0.240	2.34	8530	5470
10	05238−0626	7380	183	464	0.040	0.56	9310	10 700
11	05341+0852	7060	210	323	0.090	4.12	7420	5620
13	05381+1012	4850	183	377	0.072	0.26	9910	11 900
18	06338+5333	6250	267	167	0.002	0.00	5810	5860
19	06530−0213	7700	182	480	0.129	5.40	4880	3260
21	07131−0147	3330	171	371	0.554	1.74	13 900	19 200
22	07171+1823	13 600	203	488	0.111	0.00	22 800	22 000
23	07253−2001	6900	206	335	1.270	0.00	22 300	27 500
24	07430+1115	4850	201	300	0.242	2.51	7460	8570
25	08187−1905	6630	135	937	0.168	0.38	5070	4540
26	23304+6147	5200	173	453	0.366	4.33	4880	4310

[a] Same values in Table 3.
[b] Correspond to mass-loss rate $\dot{M}$ ($= M_{\rm dust+gas} \times 10^{-4}\ M_\odot\ {\rm yr}^{-1}$).
[c] Interstellar extinction derived from the model fitting.
[d] Derived distances using the model fitting ($L = 8000\ L_\odot$) .
[e] Derived distances assuming $M_V = M_{\rm bol,8000\odot}$−B.C.

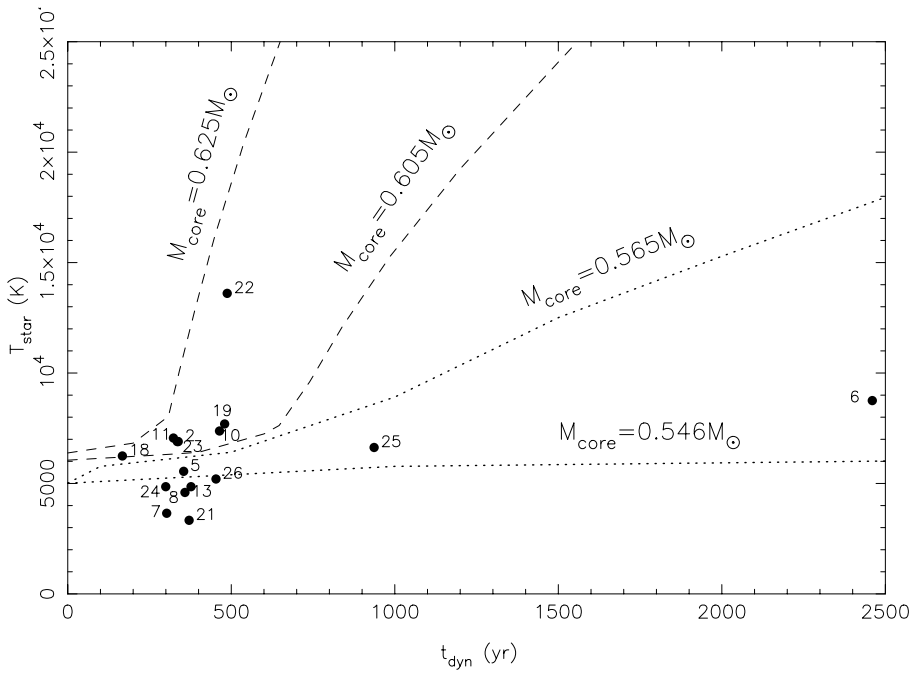

Fig. 7. Comparison of the stellar temperature with dynamical time of the dust shell, assuming constant expansion velocity ($15\,{\rm km\,s^{-1}}$). Dashed and dotted lines are theoretical evolution of hydrogen-burning post-AGB models with core mass 0.546–0.625 $M_\odot$. The dashed lines are cited from Blöcker (1995) and the dotted lines are cited from Schönberner (1983).

In Fig. 7, two stars exist apart from the main group. One is IRAS 05040+4820 and the other is IRAS 08187−1905. In spite of their relatively low stellar temperatures, the dynamical ages of their dust shells are large. These dust shells most likely will disperse into the interstellar space before the stellar temperature rises to ionize the surrounding gases. We note that they are on the evolutionary track of $M_{\rm core} = 0.55\ M_\odot$ indicating low mass for their parent stars, probably one solar mass or less. Renzini (1981) predicted the fate of a low mass star to become a white dwarf bypassing the PN stage. Scarcity of PNe in globular clusters supports his hypothesis, but

no direct evidence has been found as far as we know. The above two IRAS sources are the first sample of Renzini's "lazy" AGB remnants.

4.2. Notes on individual objects

IRAS 02086+7600

It is a member of the dark cloud L1333, which is a molecular cloud in Cassiopeia (Obayashi et al. 1998). It is identified with CO core No. 4 and is most likely a young stellar object (YSO) embedded in a CO core. The far-infrared luminosity of this source was estimated to be about 1 $L_{\odot}$ at a distance of 180 pc. The 12 μm to 25 μm flux ratio is significantly smaller than that of a typical T Tau star.

Van de Steene & Pottasch (1995) considered it as a possible planetary nebula, however they have not found radio continuum emission from this source. Slysh et al. (1994) searched for OH maser emission and it was detected at 1667 and 1665 MHz with a velocity of 3.1 km s^{-1}. Preite-Martinez (1988) considered it as a possible new PN. It may be a ultra-compact H II region, or a post-AGB star, or a YSO. We need $BVRI$ observations and a low resolution spectrum to understand the evolutionary stage of this object.

IRAS 02143+5852

Manchado et al. (1989) and García-Lario et al. (1997) made JHK photometric observations and our JHK photometric magnitudes are in agreement with theirs. Omont et al. (1993) considered it as a carbon-rich PPN, however no CO and HCN emission is detected. It is a F type post-AGB supergiant (Meixner et al. 1999). Meixner et al. (1999) imaged it at 11.7 μm and it is not resolved.

IRAS 02528+4350

Because of its IRAS colors, it was classified as a post-AGB candidate. However, Nakanishi et al. (1997) recently found it to be a galaxy with a redshift of 33 678 km s^{-1}. Crawford et al. (1996) also consider it as an ultraluminous infrared galaxy, however no radio emission is detected. The JHK photometric observations of Manchado et al. (1989), García-Lario et al. (1997) are in agreement with ours. They and Van de Steene & Pottasch (1995) considered it as a PPN/PN. However in the light of recent work of Nakanishi et al. (1997), it is a galaxy and not a post-AGB star.

IRAS 04269+3550

Van de Steene & Pottasch (1995) considered it as a PN candidate, however they did not detect radio continuum emission. Wouterloot et al. (1993) searched for H_2O, OH, CH_3OH and CO and did not detect any of these emissions. Preite-Martinez (1988) considered it as a possible new PN. From our JHK photometry and IRAS data, the SED of this object seems to be a single peaked curve rather than a double peaked curve. It maybe a post-AGB star obscured by the thick dust-shell. To confirm the object type, we need other observations, such as spectroscopy.

IRAS 04296+3429

The unidentified emission feature at 21 μm was first discovered in the IRAS LRS spectra of four carbon-rich post-AGB stars (Kwok et al. 1989), including IRAS 04296+3429. It also possesses a strong 30 μm emission (Szczerba et al. 1999). In the optical spectrum emission bands (0, 0) and (0, 1) of the Swan system of the C_2 molecule were detected (Klochkova et al. 1999). The effective temperature of the star from high resolution spectrum was estimated to be 6300 K. The star is metal-poor ([Fe/H]= -0.9) and overabundant in carbon and s-process elements (Decin et al. 1998; Klochkova et al. 1999), van Winckel & Reyniers (2000) similar to that of other 21 μm post-AGB stars such as IRAS 05341+0852 (Reddy et al. 1997).

IRAS 05113+1347

It is a 21 μm carbon-rich post-AGB star (Kwok et al. 1995). It shows C_2, C_3 and 11.3 μm emission features.

IRAS 05170+0535

Van den Ancker et al. (1998) classified it as a low mass young stellar object. Coulson et al. (1998) considered it as a Vega-excess star. The G0Ve spectrum and Hipparcos parallax suggests that it is not a post-AGB star. It is most likely a young G dwarf at the end of the T Tauri phase. The Hipparcos parallax yields a distance of 180 pc and a luminosity of about 1.23 $L_{\odot}$.

IRAS 05238−0626

Its spectral type is F2II (Reddy & Parthasarathy 1996). The photometric observations made by García-Lario et al. (1997) and Torres et al. (1995) are in agreement with our observations.

IRAS 05341+0852

It is a post-AGB star with 21 μm emission. Reddy et al. (1997), van Winckel & Reyniers (2000) found it to be metal-poor and overabundant in carbon and s-process elements. It appears to have evolved from the AGB carbon star stage to post-AGB stage only recently. Our $BVRI$ data of this star is in good agreement with the photometric data of Hrivnak & Kwok (1999). However, our JHK data differ by about 0.2 mag from the JHK data reported by Hrivnak & Kwok (1999). They classified the low resolution spectrum of this star and assigned a spectral type G2 0-Ia.

IRAS 05355−0117

Its optical counterpart is HD 290764. Its spectral type is A5III (Schild & Cowley 1971). It is considered as a δ Scuti star with a full amplitude of 0.016 mag. However, the presence of cold detached dust shell is

not consistent with the δ Scuti type variability. It is likely a pre-main-sequence star in the Orion stellar ring. High resolution spectroscopic analysis may help us to understand the evolutionary stage of this star.

IRAS 06013−1452

It is a high galactic latitude Ae star. Thé et al. (1994) listed it in the catalog of Herbig Ae/Be stars. García-Lario et al. (1997) also classified it as a Herbig Ae/Be star.

IRAS 06059−0632

It is a B3 star in the direction of Orion OB1 association (de Geus et al. 1990). It is listed in the Hipparcos cataloge ($\pi = 1.68$ mas). This source is probably a nearby pre-main-sequence star and not a post-AGB supergiant.

IRAS 06060+2038

It is a low galactic latitude IRAS source with B1V star in the direction of Gemini OB1 molecular cloud complex. It is in the Sharpless 252 which is an extended H II region (Haikala 1994).

IRAS 06284−0937

Van den Ancker et al. (1998) considered it as a Herbig Ae/Be star. It is in the Hipparcos cataloge ($\pi = 4.6$ mas). It may be a variable star (NSV 2998).

IRAS 07077−1825

It is a O6 star listed in the LS catalog as LS 207 (Reed & Beatty 1995) and is in the direction of the Sharpless 301 which is an extended H II region (Moffat et al. 1979).

IRAS 07131−0147

It is a bipolar object with a M5III central star (Scarrott et al. 1990). The evolutionary status of this star is not clear. The M5III spectral type suggests that it may be a first ascent red giant and may not be a post-AGB star.

IRAS 07171+1823

It is found to be very low excitation planetary nebula with a hot (B-type) post-AGB central star (Vijapurkar et al. 1998). It shows nebular emission lines of [N II] and [S II]. The Balmer lines are also in emission. It is a high galactic latitude hot-post-AGB star.

IRAS 07430+1115

It is a high galactic latitude carbon-rich post-AGB star (Hrivnak & Kwok 1999). Our $BVRI$ photometry of this star is in agreement within 0.25 mag with the photometric data reported by Hrivnak & Kwok (1999). The difference may be due to small amplitude light variations of this star.

5. Conclusions

From the $BVRIJHK$ photometry of 27 IRAS sources with far-infrared colors similar to planetary nebulae, 17 objects are found to be most likely post-AGB stars. From the analysis of SED we have obtained some of the parameters of their circumstellar dust shells. We plotted our objects on the diagram of the stellar temperature against the dynamical time of the dust shell. Comparing with the theoretical evolutionary tracks of the post-AGB stars, two objects are classified as slowly evolving post-AGB stars which may evolve into white dwarfs without experiencing the PNe phase.

Acknowledgements. We would like to thank Dr. B. J. Hrivnak for careful reading of this manuscript and valuable comments. We used the SIMBAD database operated at CDS, Strasbourg, France. M.P. thanks Prof. Keiichi Kodaira, Prof. Shuji Deguchi, Prof. Norio Kaifu and Prof. Hiroshi Karoji for their kind encouragement, support and hospitality.

References

Blöcker, T. 1995, A&A, 299, 755
Burstein, D., & Heiles, C. 1982, AJ, 87, 1165
Coulson, I. M., Walther, D. M., & Dent, W. R. F. 1998, MNRAS, 296, 934
Cox, A. N. (ed.) 2000, Allen's Astrophysical Quantities, 4th ed. (New York: Springer)
Crawford, T., Marr, J., Partridge, B., & Strauss, M. A. 1996, ApJ, 460, 225
Decin, L., van Winckel, H., Waelkens, C., & Bakker, E. J. 1998, A&A, 332, 928
de Geus, E. J., Lub, J., & van de Grift, E. 1990, A&AS, 85, 915
Elias, J. H., Frogel, J. A., Matthews, K., & Newgebauer, G. 1982, AJ, 87, 1029
García-Lario, P., Manchado, A., Pottasch, S. R., Suso, J., & Olling, R. 1990, A&A, 82, 497
García-Lario, P., Manchado, A., Pych, W., & Pottasch, S. R. 1997, A&AS, 126, 479
Glass, I. S., & Feast, M. W. 1982, MNRAS, 198, 199
Hardorp, J., Rohlfs, K., Slettebak, A., & Stock, J. 1959, in Luminous Stars in the Northern Milky Way (Hamburg-Bergedorf)
Haikala, L. K. 1994, A&AS, 108, 643
Hu, J. Y., te Lintel Hekkert, P., Slijkhuis, S., et al. 1994, A&AS, 103, 301
Hrivnak, B. J., Kwok, S., & Volk, K. M. 1989, ApJ, 346, 265
Hrivnak, B. J. 1995, ApJ, 438, 341
Hrivnak, B. J., & Kwok, S. 1999, ApJ, 513, 869
Itoh, N., Yanagisawa, K., Ichikawa, T., Tarusawa, K., & Ќataza, H. 1995, in Proceedings of SPIE Symp., 2552, 430
Klochkova, V. G., Szczerba, R., Panchuk, V. E., & Volk, K. 1999, A&A, 345, 905
Kwok, S., Volk, K., & Hrivnak, B. J. 1989, ApJ, 345, L51
Kwok, S., Hrivnak, B. J., & Geballe, T. R. 1995, ApJ, 454, 394
Landolt, A. U. 1992, AJ, 104, 340
Manchado, A., Pottasch, S. R., García-Lario, P., Esteban, C., & Mampaso, A. 1989, A&A, 214, 139
Meixner, M., Ueta, T., Dayal, A., et al. 1999, ApJS, 122, 221
Moffat, A. F. J., Fitzgerald, M. P., & Jackson, P. D. 1979, A&AS, 38, 197
Nakanishi, K., Takata, T., & Yamada, T. 1997, ApJS, 112, 245
Neckel, Th., & Klare, G. 1980, A&AS, 42, 251

Obayashi, A., Kun, M., Sato, F., Yonakura, Y., & Fukui, Y. 1998, AJ, 115, 274
Omont, A., Loup, C., Forveille, T., et al. 1993, A&A, 267, 515
Parthasarathy, M., & Pottasch, S. R. 1986, A&A, 154, L16
Parthasarathy, M., & Pottasch, S. R. 1989, A&A, 225, 521
Parthasarathy, M. 1993, in Luminous High-Latitude Stars, ed. D. Sasselov, ASP Conf. Ser., 45, 173
Pottasch, S. R., Bignell, C., Olling, R., & Zijlstra, A. A. 1988, A&A, 205, 248
Preite-Martinez, A. 1988, A&AS, 76, 317
Reed, B. C., & Beatty, A. E. 1995, ApJS, 97, 189
Reddy, B. E., & Ṕarthasarathy, M. 1996, AJ, 112, 2053
Reddy, B. E., Parthasarathy, M., Gonzalez, G., & Bakker, E. J. 1997, A&A, 328, 331
Renzini, A. 1981, in Physical Processes in Red Giants, ed. I. Iben, & A. Renzini (Dordrecht:Reidel), 431
Rieke, G. H., & Lebofsky, M. J. 1985, ApJ, 288, 618
Scarrott, S. M., Rolph, C. D., Wolstencraft, R. D., Walker, H. J., & Sekiguchi, K. 1990, MNRAS, 245, 484
Schechter, P. L., Mateo, M., & Saha, A. 1993, PASP, 105, 1342
Schild, R. E., & Ćowley, A. P. 1971, A&A, 14, 66
Schlegel, D. J., FiKbeiner, D. P., & Davis, M. 1998, ApJ, 500, 525
Schmidt-Kaler, Th. 1982, in Landolt-Börnstein: Numerical Data and Functional Relationships in Science and Technology, vol. 2b, ed. K. Schaifers, & H. H. Voigt (Springer-Verlag, Berlin)
Schönberner, D. 1983, ApJ, 272, 708
Schönberner, D. 1989, in Planetary Nebulae, ed. S. Torres-Peimbert, IAU Symp., 131, 463
Schönberner, D., & Blöcker, T. 1993, in Luminous High-Latitude Stars, ed. D. Sasselov, ASP Conf. Ser., 45, 337
Slysh, V. I., Dzura, A. M., Valtts, I. E., & Gerard, E. 1994, A&AS, 106, 87
Szczerba, R., Henning, Th., Volk, K., Kwok, S., & Cox, P. 1999, A&A, 345, L39
Thé, P. S., de Winter, D., & Pérez, M. R. 1994, A&AS, 104, 315
Torres, C. A. O., Quast, G., de La Reza, R., Gregorio-hetem, J., & Lepine, J. R. D. 1995, AJ, 109, 2146
van den Ancker, M. E., de Winter, D., & Tjin A Djie, H. R. E. 1998, A&A, 330, 145
van der Veen, W. E. C. J., & Habing, H. J. 1988, A&A, 194, 125
van der Veen, W. E. C. J., Habing, H. J., & Geballe T. R. 1989 A&A, 226, 108
van Winckel, H., & Reyniers, M. 2000, A&A, 354, 135
Vijapurkar, J., Parthasarathy, M., & Drilling, J. S. 1998, Bull. Astr. Soc. India, 26, 497
Van de Steene, G. C., & Pottasch, S. R. 1995, A&A, 299, 238
Whitelock, P. A. 1985, MNRAS, 213, 59
Wouterloot, J. G. A., Brend, J., & Fiegle, K. 1993, A&AS, 98, 589
Zuckerman, B., Forveille, T., & Kastner, J. H. 1995, Nature, 373, 494